Original Article

Institution of MECHANICAL ENGINEERS
Journal of ENGINEERING IN MEDICINE

Proc IMechE Part H:
J Engineering in Medicine
2014, Vol. 228(9) 971–982

DOI: 10.1177/0954411914551854
pih.sagepub.com
SAGE

Hip joint centre position estimation using a dual unscented Kalman filter for computer-assisted orthopaedic surgery

Elisa Beretta[1], Elena De Momi[1], Valentina Camomilla[2], Andrea Cereatti[3], Aurelio Cappozzo[2] and Giancarlo Ferrigno[1]

Abstract

In computer-assisted knee surgery, the accuracy of the localization of the femur centre of rotation relative to the hip-bone (hip joint centre) is affected by the unavoidable and untracked pelvic movements because only the femoral pose is acquired during passive pivoting manoeuvres. We present a dual unscented Kalman filter algorithm that allows the estimation of the hip joint centre also using as input the position of a pelvic reference point that can be acquired with a skin marker placed on the hip, without increasing the invasiveness of the surgical procedure. A comparative assessment of the algorithm was carried out using data provided by *in vitro* experiments mimicking in vivo surgical conditions. Soft tissue artefacts were simulated and superimposed onto the position of a pelvic landmark. Femoral pivoting made of a sequence of star-like quasi-planar movements followed by a circumduction was performed. The dual unscented Kalman filter method proved to be less sensitive to pelvic displacements, which were shown to be larger during the manoeuvres in which the femur was more adducted. Comparable accuracy between all the analysed methods resulted for hip joint centre displacements smaller than 1 mm (error: 2.2 ± [0.2; 0.3] mm, median ± [inter-quartile range 25%; inter-quartile range 75%]) and between 1 and 6 mm (error: 4.8 ± [0.5; 0.8] mm) during planar movements. When the hip joint centre displacement exceeded 6 mm, the dual unscented Kalman filter proved to be more accurate than the other methods by 30% during multi-planar movements (error: 5.2 ± [1.2; 1] mm).

Keywords

Hip joint centre, unscented Kalman filter, computer-assisted orthopaedic surgery, soft tissue artefact

Date received: 12 April 2014; accepted: 27 August 2014

Introduction

The hip joint centre (HJC) localization has great importance for lower limb movement analysis,[1,2] for hip tissue's contact evaluation with three-dimensional (3D) computer-based simulations[3] and for the correct alignment of prosthetic components in orthopaedic surgery.[4–6] To this end, since the hip joint behaves as a ball-and-socket joint,[7] functional methods identify the HJC as the unique centre of rotation of the femur relative to the hip-bone during ad hoc pivoting movements.[8–10] Although the functional HJC localization method entails tracking the movement of both the bone segments involved (i.e. the femur and the pelvis), in some computer-assisted orthopaedic surgery (CAOS) applications, for example, during total knee replacement, the pelvic pose is not tracked[11] and the HJC is estimated by tracking only the movement of the femur. The HJC is the centre of rotation of this bone relative to a fixed frame, therefore under the hypothesis of an absence of pelvic motion.

One of the frequently adopted HJC estimation methodologies for clinical use in CAOS[12,13] is the minimal amplitude point (MAP) method.[14] The performance of this method was assessed in several studies, but none of

[1]Department of Electronics, Information and Bioengineering, Politecnico di Milano, Milan, Italy
[2]Department of Movement, Human and Health Sciences, Università degli Studi di Roma Foro Italico, Rome, Italy
[3]Department of Information Engineering, Political Sciences and Communication Sciences, Università degli Studi di Sassari, Sassari, Italy

Corresponding author:
Elisa Beretta, Department of Electronics, Information and Bioengineering, Politecnico di Milano, p.zza Leonardo da Vinci 32, 20133 Milan, Italy.
Email: elisa.beretta@polimi.it

them investigated the relation between the HJC localization accuracy and the passive pelvic displacement in a realistic experimental set-up. Stindel[13] simulated the pelvic motion by adding a random error (maximum amplitude of 16 mm) to a reference stationary HJC position. The error in the HJC position localization was proportional to the pelvic displacement and the femoral axis estimation deviated by a maximum of 1°. Lustig et al.[15] simulated pelvic movements of different amplitudes using a physical model that mimicked the femur and the hip joint. When the pelvic movement amplitudes were around 15 mm, the HJC localization error was approximately 12 mm. In Picard et al.,[12] an *in vitro* set-up with whole-body cadavers was used to mimic the operating room conditions during total knee replacement surgery. A maximal femoral axis deviation equal to 1.3°, corresponding to a HJC localization error of approximately 8 mm, was found. However, the amplitude of the pelvis displacement was not reported.

Other algorithms were comparatively assessed using a cadaveric set-up,[16–18] but the influence of the pelvic motion on the HJC localization accuracy was not investigated. In Lopomo et al.,[17] hemi-corpses constrained to the working table by means of a wooden support were used. The root mean square residual displacement of the origin of the pelvic marker-cluster, mounted on the homolateral iliac crest, was 3.5 mm. A coordinate transformation method, the so-called pivoting method,[19] was shown to be more accurate than the least-squares sphere fitting method[20] (HJC localization errors equal to 2.7 ± 2.9 and 25.2 ± 18.9 mm (mean $\pm$ standard deviation (SD))). Mihalko et al.[18] reported HJC localization errors up to 33 mm using the sphere fitting method, when the passive manoeuvres were executed on whole-body cadavers partially constrained to the working table with a belt positioned around the lower torso. The description of the employed algorithm and of the amplitude of the actual pelvic motion recorded during the pivoting manoeuvre was not provided.

Recently, De Momi et al.[21] proposed the application of a skin marker on the pelvis of the subject in order to use the partial information on the hip-bone displacements during the pivoting manoeuvres, without increasing surgical intervention invasiveness. This functional HJC localization method used the unscented Kalman filter (UKF) based on the joint-estimation filtering approach.[22] The evaluation, performed on a hip phantom with pin cluster markers, proved that for pelvic displacements between 8 and 13 mm, the UKF algorithm was able to increase the accuracy of the HJC localization (the median HJC localization error was about 12 mm) by up to 50% with respect to coordinate transformation methods.[16,19] However, the UKF method requires a time-consuming fine tuning of the Kalman filter parameters.

The aim of this study is to comparatively assess the performance of state-of-the-art HJC localization methods with respect to the passive pelvic displacement, using whole-body cadavers in an experimental set-up reproducing the operating room conditions during surgical interventions. Moreover, a new method is proposed for estimating the HJC location using a dual unscented Kalman filter (dUKF) algorithm, whose inputs are the reconstructed femoral pose and the position of a skin marker located on the pelvis. In order to overcome the above-mentioned tuning issue of the UKF joint filtering approach and enhance the estimation of the HJC position, the dUKF method implements the dual filtering technique,[23] which distinguishes between the state and parameter vector estimations in a pair of distinct sequential filters, combined with a global optimization process to adapt the Kalman gains of the parameter filter. Since a skin marker placed on the pelvis is not included in the current surgical scenario, the position of a pelvic anatomical point, identified once with a calibration procedure, was used as the observed pelvic point with simulated soft tissue artefacts (STAs). The dUKF method was compared to the MAP algorithm,[14] which is one of the most frequently adopted methods for HJC estimation in clinical use for CAOS procedures,[12,13] and to the pivoting coordinate transformation algorithm.[19] Both methods use only the femoral poses as input. Additionally, the performance of the UKF algorithm,[21] which uses both the femoral poses and the positions of the pelvic point, was assessed. The HJC position was further estimated as the centre of the best fitting sphere described by the trajectory of the pelvic point in the femoral technical frame. The robustness of the performance of these methods with respect to the pelvic displacement was also investigated.

Methods

The hip kinematic model

The hip was modelled as a spherical joint linking two rigid segments: femur and hip-bone.[21] As shown in Figure 1, the description of the kinematic chain requires the definition of the following:

- The laboratory technical frame (TF_L);
- The femur technical frame (TF_F), with the origin centred in an arbitrary distal point of the femur;
- The hip technical frame (TF_H), with the origin centred in the centre of the acetabulum and the axes oriented as the TF_F;
- An arbitrary point (A) fixed with the pelvis.

The following kinematic relationships are defined:

- The transformation from the TF_L to the TF_H (${}^H\mathbf{T}_L$), represented by the translation vector ${}^H\mathbf{c}_L$ and by the rotation vector, using a unit quaternion-based rotation representation ${}^H\mathbf{q}_L$;
- The translation vector from the TF_H to the pelvic point A (${}^A\mathbf{c}_H$), represented in spherical coordinates;
- The translation vector from the TF_F to the origin of the TF_H (${}^H\mathbf{c}_F$).

dUKF

The dUKF algorithm for HJC localization requires the femoral poses and the positions of the pelvic point during pivoting movements. The algorithm is based on the dual filtering approach[23] that intertwines a pair of distinct sequential filters for state and parameter estimation, that is, the state vector is estimated using the current parameter values and the parameters are estimated using the current state values. The time-invariant variables of the hip kinematic model, that is, the HJC position in the TF_F ($^H\mathbf{c}_F$) and the distance between the HJC and the point A of the pelvis (norm of the vector $^A\mathbf{c}_H$), are embedded in the parameter vector, while the state of the hip system is described using a first-order discrete model. Both the state and the parameter estimation steps are computed using a Kalman filter based on the unscented transform.[24] The simulated annealing method[25] is used to adapt the Kalman gain during the parameter filtering process. Moreover, a global optimization process allows exploration of the parameter space and enhancement of the HJC estimation. The dUKF algorithm is initialized using the HJC position in the TF_F estimated with the method proposed in Siston and Delp.[19] Details about the implemented dUKF method are described in Appendix 1.

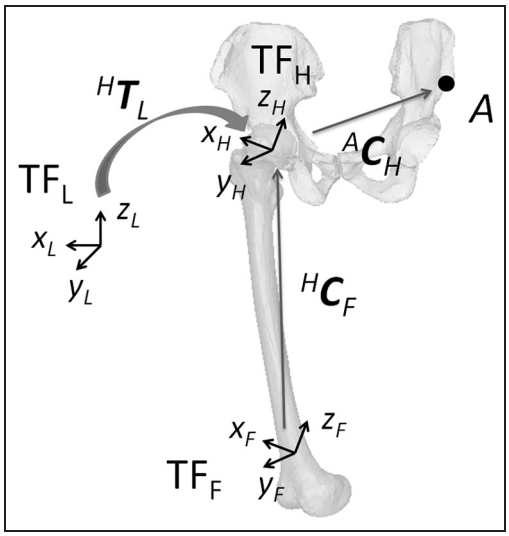

Figure 1. The hip kinematic model.

Algorithm validation

Experimental protocol. In this study, four fresh intact adult cadavers, with no evidence of damage to the hip joints, were used.[26] The cadavers lied supine on an operating table without any fixating support. For each cadaver, one transosseous steel pin (6 mm in diameter) was fixed distal to the right femur and one into the left hip-bone (Figure 2(a)). Each pin was equipped with a four-marker cluster. The minimum distance between two markers of the same cluster was 70 mm. Prior to inserting the pins into the bones, cruciform incisions were made through the skin and soft tissue to reduce forces applied to the pins. A 9-camera VICON MX close-range stereophotogrammetric system (VICON, Oxford, UK) was used to acquire (at 120 frame/s) the instantaneous position of the markers. As reported in Cereatti et al.,[26] the accuracy of the VICON system in estimating the centre of rotation of a mechanical linkage that mimicked the geometry of the pelvis and femur ensemble was 0.7 mm (SD = 0.2 mm). The following anatomical landmarks were calibrated with an optical pointer: right and left anterior superior iliac spines (ASISs) and posterior superior iliac spines (PSISs) and lateral and medial epicondyles. Three trials were performed for each cadaver while an operator manually moved the right femur with respect to the hip-bone.

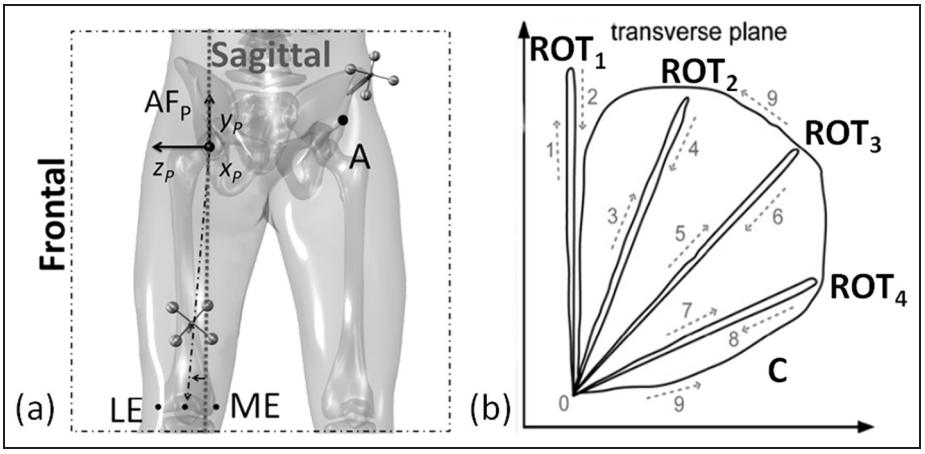

Figure 2. (a) Schematic for the experimental set-up: a pin marker-cluster was drilled into the femur and hip-bone of the cadaver. The pelvic anatomical frame (AF_P) together with the pelvic point (A) and the projection of the mean point between the lateral epicondyle (LE) and the medial epicondyle (ME) on the frontal plane are indicated. (b) Trajectory of the lateral epicondyle during the hip joint movement projected onto the pelvic transverse plane quasi-orthogonal to the operating table. The starting position is indicated by 0, the direction of progression is shown by the arrows (1–9) during the execution of phases $ROT_{1,2,3,4}$ and C.

A *StarArc* movement[8] was performed for each trial. It consisted of the following phases (Figure 2(b)): a flexion–extension in the sagittal plane (ROT_1), a composition of flexion–extension and adduction–abduction in three planes externally rotated about the cranio-caudal axis by about 20°, 40°, and 60° ($ROT_{2,3,4}$), respectively, followed by a half circumduction, C.

Model of the pelvic STA. Since a skin marker on the pelvis was not available during the experiments, the position of the calibrated left ASIS, which was contralateral with respect to the moving femur, was taken as the arbitrary observed pelvic point (point A of the hip kinematic model in Figure 1), where the STAs[27] are expected to be minimal. The STA on the observed point A was simulated as a joint kinematic–driven noise, following a similar approach to that proposed and validated in a previous study for markers placed on the thigh.[28] The simulated noise was added to the position of the contralateral ASIS ($^A\mathbf{c}_P$) in the pelvic anatomical system of reference (see section 'Data analysis'), which is given as follows

$$^A\tilde{\mathbf{c}}_P(t) = {}^A\mathbf{c}_P + \frac{a}{2}\cdot\Sigma\cdot\mathbf{v} \quad \text{with } |\Sigma_{ij}| < 1 \tag{1}$$

where $\mathbf{v} = [\alpha, \beta, \gamma]$ is the vector of the hip joint angles (see section 'Data analysis'), a is a positive scalar value defining the maximum amplitude of the simulated noise, and Σ is the full matrix of the normalized correlation coefficients. Subsequently, the noisy trajectory $^A\tilde{\mathbf{c}}_P$ is expressed in the TF_L to be used as the observations of the pelvic point A for the HJC estimation. The maximum amplitude of the simulated STA was set equal to 5 mm, as discussed in section 'Discussion', while the elements of the correlation matrix Σ_{ij} were sampled from a uniform distribution in the range between -1 and 1, for each trial and each cadaver.

Data analysis. The femur (TF_F) and pelvic technical frame (TF_P) poses relative to the global system of reference were estimated using a single value decomposition technique.[29] The pelvic anatomical system of reference (AF_P) was determined according to the definitions proposed in Cappozzo et al.[30] and was registered relative to the TF_P (Figure 2(a)).

An estimate of the hip joint angles was obtained from the projections of the vector identified by the mean point between the positions of the lateral and the medial epicondyles and the HJC onto the relevant plane of the AF_P (α flexion–extension in the sagittal plane, β adduction–abduction in the frontal plane, and γ internal–external rotation in the transverse plane).

In each movement phase ($ROT_{1,2,3,4}$ and C), the maximum hip angular displacement (range of motion (ROM)) was computed. For each cadaver, the reference HJC position in the TF_F ($^H\mathbf{c}_F$) was estimated using the functional pivoting method[19] and the dataset of the pelvic and femoral poses obtained from the corresponding pin-marker-based TFs. In order to quantify the pelvic motion occurring during the passive manoeuvres, the displacement d was computed as the norm of the ellipsoidal axes estimated on the trajectory of the reference HJC in the TF_L through the principal component analysis technique.[31] All recorded *StarArc* trials were split into $ROT_{1,2,3,4}$ and C movement phases, and for each of them, the displacement d was computed. For all phases, the median HJC displacement (d_m) and the first and third inter-quartile ranges (IQRs; from 50% to 25% and 75%, respectively), over all specimens and trials, were computed. A comparative analysis of the pelvic displacement occurring during the different movement phases was carried out using the Kruskal–Wallis test with Bonferroni–Holm correction ($p < 0.05$). Then, each movement phase dataset was clustered into three datasets according to the amplitude of the HJC displacement d: small (< 1 mm), medium (between 1 and 6 mm) and large (> 6 mm).

For each cadaver and for each trial, the HJC location in the TF_F was estimated using the dataset associated with each of the movement phases ($ROT_{1,2,3,4}$ and C) and with the whole *StarArc* movement, using the following methods:

1. *MAP*: the minimal amplitude point method,[14] using the instantaneous TF_F poses;
2. *PIV*: the pivoting method,[19] using the instantaneous TF_F poses;
3. *UKF*: the unscented Kalman filter method,[21] using the instantaneous TF_F poses and the positions of the simulated pelvic point A expressed in the TF_L;
4. *dUKF*: the dual unscented Kalman filter method, using the instantaneous TF_F poses and the positions of the simulated pelvic point A expressed in the TF_L.

Moreover, for each cadaver and each trial, another HJC estimation method was applied to the dataset associated with the whole *StarArc* movement:

5. *PSF:* the closed-form sphere fitting method,[20] using the instantaneous positions of the simulated pelvic point A expressed in the TF_F.

The accuracy of the methods 1–5 was assessed by computing the Euclidean distance between the estimated ($^H\hat{\mathbf{c}}_F$) and the reference ($^H\mathbf{c}_F$) HJC position in the TF_F. In this way, the errors due to the manually performed anatomical calibration procedure do not affect the computation of the accuracy index. For each method, the median errors and the first and third IQRs (25% and 75%, respectively), over specimens and trials, were computed. A comparative analysis of the performance of the dUKF, PSF, PIV, MAP and UKF algorithms was carried out using the Friedman paired test with Bonferroni–Holm correction ($p < 0.05$).

To assess whether the HJC localization accuracy correlated with the pelvic displacement, the Pearson

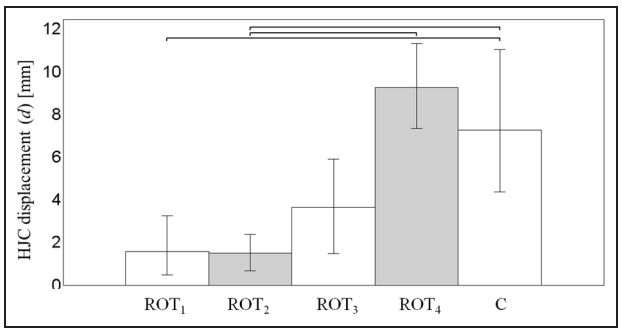

Figure 3. Evaluation of the displacement (d) in the laboratory frame of the reference HJC as occurring during the different phases of the passive *StarArc* pivoting motion ($ROT_{1,2,3,4}$ and C). Vertical bars represent median values and quartiles (25% and 75%) for each HJC displacement population. Horizontal lines represent statistically significant differences as determined in intra-group comparisons (Kruskal–Wallis test, $p < 0.05$) with Bonferroni–Holm correction.
HJC: hip joint centre.

Table 1. The median values of the maximum hip angular displacement (ROM) and the HJC displacement (d) computed in each phase and on the whole *StarArc* movement, averaged over the trials of all cadavers.

	Median ROM (°)	d (mm)		
		Min	Max	Median
ROT_1	48.8	0.2	8.3	1.6
ROT_2	46.9	0.1	5.6	1.5
ROT_3	42.2	0.7	11.2	3.6
ROT_4	36.7	0.1	14.7	9.3
C	48.2	1.1	13.8	7.3
StarArc	49.2	0.9	9.2	6.8

ROM: range of motion.

correlation analysis ($p < 0.05$) between the HJC localization errors and the HJC displacement d was carried out on the single motion phases. The relationship between d and the maximum hip angular displacement ROM was also investigated.

Results

The maximum hip angular displacements for each phase of the *StarArc* manoeuvre and the corresponding HJC displacements are reported in Table 1. The comparative analysis performed on HJC displacements in each hip motion phase is shown in Figure 3. On average, the largest pelvic displacements occurred during ROT_4 (median displacement equal to 9.3 mm) and C (median displacement equal to 7.3 mm). The HJC localization errors for the different motion phases of the *StarArc* movement, averaged over specimens and trials, are reported in Figure 4 for all the tested methods.

The dUKF method exhibited the smallest median HJC localization error both in the whole *StarArc* motion and in the motion phases ROT_4 and C, during which the median HJC displacement d is >6 mm, while it showed a comparable localization accuracy in the other cases. When the whole *StarArc* motion was used to determine the HJC (Figure 4), the dUKF method ($5.2 \pm [1.2;\ 1]$ mm, median $\pm$ [IQR 25%; IQR 75%]) was shown to be more accurate than the MAP method ($9.5 \pm [0.7;\ 0.7]$ mm). The accuracy of the dUKF method was about 30% higher than the accuracy of PSF method ($9.2 \pm [3.2;\ 6.2]$ mm), PIV ($7.9 \pm [2.5;\ 0.4]$ mm) and UKF ($8.7 \pm [2.8;\ 2.3]$ mm) methods, although no significant differences were computed.

When data relative to the circumduction movement were used (C), the median HJC localization errors of all the analysed methods were below 10 mm. Besides the fact that the median HJC localization errors between all methods differed by <4 mm, the accuracy of the dUKF method ($6.9 \pm [0.9;\ 1.6]$ mm) was significantly greater than the accuracies of the MAP and the UKF methods. A 40% reduction of the median HJC localization error of the dUKF method with respect to the other methods was computed during the ROT_4 planar motion, although the only statistically significant difference resulted with respect to the MAP method.

In Figure 5, HJC localization errors relative to the three pelvic displacement datasets (small, medium and large) are shown for all methods. In case of small pelvic displacement (<1 mm), the performance of all the methods was in line with the measurement accuracy of the system (median HJC localization errors <3.5 mm). For the medium pelvic displacement dataset (between 1 and 6 mm), the accuracy of dUKF ($4.5 \pm [1.2;\ 2.3]$ mm) was significantly greater than that of the MAP method ($6.2 \pm [2.0;\ 1.3]$ mm). For large pelvic displacement dataset (>6 mm), the HJC localization errors of the dUKF method were found to be significantly reduced with respect to all the other methods analysed.

No significant differences were found between the HJC localization errors of the other methods (MAP, PIV, PSF and UKF) when considering both the HJC displacement (Figure 5) and the dataset divided by motion phases (Figure 4), except for the accuracy of the MAP method, that was shown to be significantly smaller than the accuracy of the PIV method during ROT_1.

The correlation analysis results are reported in Table 2. No significant correlation values were found between d and ROM (correlation coefficient equal to -0.2). The accuracy of all HJC estimation methods was found to be positively correlated with the HJC displacement (correlation coefficient up to 0.8); however, the correlation coefficient for the dUKF was lowest (equal to 0.5).

Discussion

The alignment of the knee prosthesis during arthroplasty procedures is considered successful when the femoral axis results in $\pm 3°$ varus-valgus after the

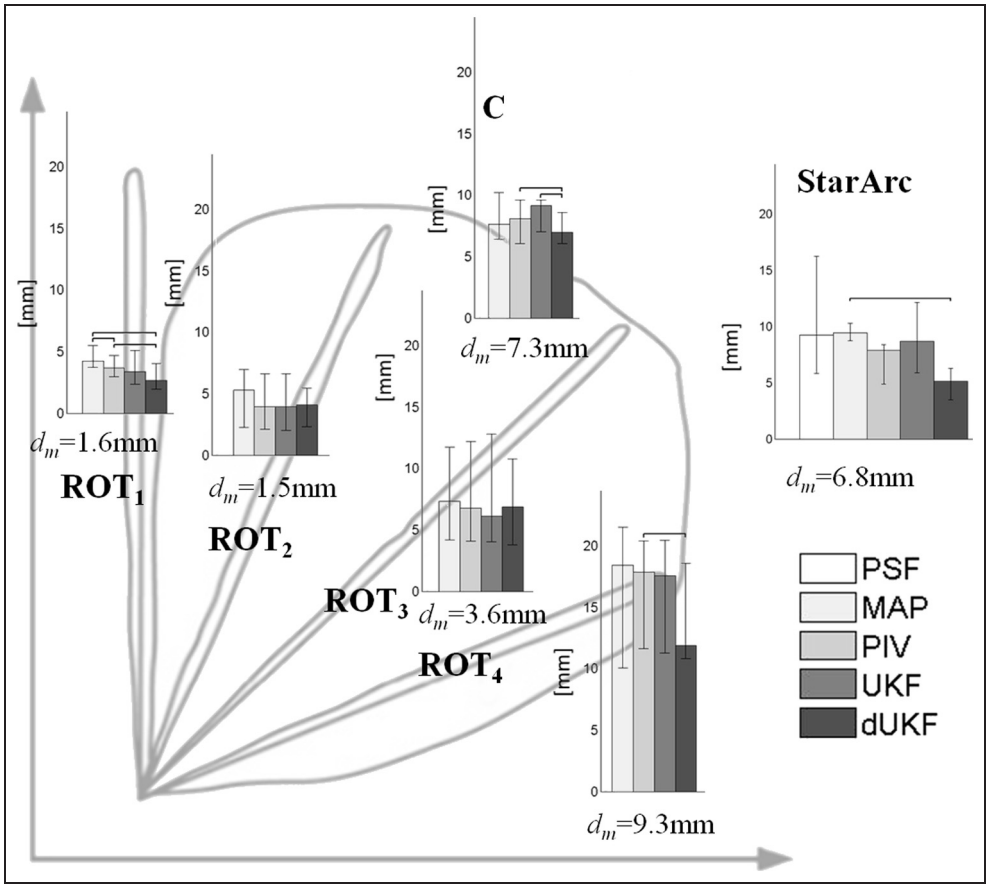

Figure 4. Evaluation of the HJC localization error using the four algorithms (PIV, MAP, UKF, and dUKF) and the datasets corresponding to the different phases of the passive *StarArc* pivoting motion ($ROT_{1,2,3,4}$ and C) and using the five algorithms (PSF, PIV, MAP, UKF and dUKF) and the datasets corresponding to the whole *StarArc* motion, for all trials of the four cadavers. Vertical bars represent median values and quartiles (25% and 75%) of each HJC localization error population. Horizontal lines represent statistically significant differences as determined in intra-group comparisons (Friedman paired test, $p < 0.05$) with Bonferroni–Holm correction. The median HJC displacement (d_m) computed for each phase is also reported.
HJC: hip joint centre; PSF: sphere fitting; MAP: minimal amplitude point; PIV: pivoting; UKF: unscented Kalman filter; dUKF: dual unscented Kalman filter.

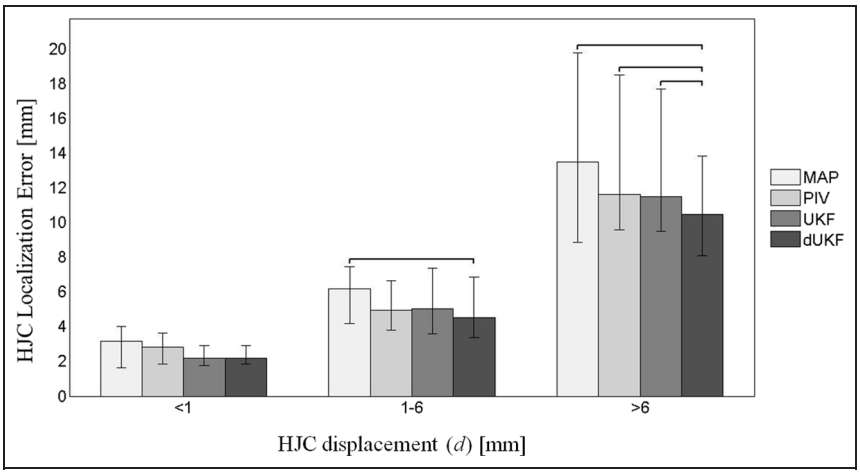

Figure 5. Evaluation of the HJC localization error using the four algorithms (PIV, MAP, UKF and dUKF) in the small (< 1 mm), medium (1–6 mm), and large (> 6 mm) HJC displacement groups, averaged over the trials of all cadavers. Vertical bars represent median values and quartiles (25% and 75%) of each HJC localization error population. Horizontal lines represent statistically significant differences as determined in intra-group comparisons (Friedman paired test, $p < 0.05$) with Bonferroni–Holm correction.
HJC: hip joint centre; MAP: minimal amplitude point; PIV: pivoting; UKF: unscented Kalman filter; dUKF: dual unscented Kalman filter.

Table 2. Pearson correlation analysis between the HJC displacement *d* and, first, the HJC localization errors of the four methods and, second, the maximum hip angular displacement ROM.

		d (mm)
HJC localization errors (mm)	MAP	0.8*
	PIV	0.7*
	UKF	0.7*
	dUKF	0.5*
ROM (°)		−0.2*

HJC: hip joint centre; MAP: minimal amplitude point; PIV: pivoting; UKF: unscented Kalman filter; dUKF: dual unscented Kalman filter; ROM: range of motion.
*Statistically significant difference ($p < 0.05$).

intervention.[4,6] The inaccuracy with which the HJC is determined is one of the factors that negatively impacts on the latter requirement,[32] and it is, therefore, important to reduce it to a minimum.[33] This study aimed at providing a contribution to this goal.

It has been shown that the current HJC estimation methods are highly influenced by the pelvic motion that might occur during the passive femoral movements.[16] In this study, we present a dUKF method for the HJC localization which partially compensates for the pelvic motion during hip pivoting movements. The method requires the knowledge of the femoral pose and of the position of a pelvic point. The HJC position in the laboratory space can be tracked under the hypothesis of motion regularity according to the Bayesian approach. Unlike the previously proposed UKF method,[21] the dual estimation approach provides the estimation of the system state and of the parameter vectors in two parallel and intertwined filtering processes, allowing the adaptation of the parameter filter gains through a simulated annealing algorithm. The computational time (in the range of 15′ and 45′ for a signal 1000 frames in length, using MatLab R2009b for computation, on a dual core central processing unit (CPU) at 3 GHz), due to the Kalman joint estimation and simulated annealing, limits the immediate clinical applicability of the approach. It has to be noted that the global optimal solution was found in the first 10 iterations for all the tests performed. Moreover, the implementation of the proposed algorithm was not optimized and it can be reduced by at least 10%.

The applicability of placing a skin marker on the patient's hip during the surgical procedure was already presented and discussed in De Momi et al.[21] The use of a tracked stick pointing to the pelvic landmark would overcome not only the sterility problem but even the visibility issue derived from the use of optical tracking system in the odds ratio. Moreover, knee CAOS procedures are usually performed with the patient lying on the bed, so that the ASISs can be easily pointed.

The performance of the proposed dual UKF method was assessed using an *in vitro* set-up with fresh cadavers that reproduced a realistic surgical scenario. The analysis conducted showed that, during the hip pivoting movements required for the HJC determination, the pelvic displacement ranged between 0.1 and 15 mm. These values were comparable with those observed in the *in vitro* analyses performed in Lustig et al.[15] and De Momi et al.[21] The largest pelvic displacements were observed during the manoeuvres that involved the largest hip abduction (ROT_4, C). This observation is explained by the compensatory pelvic motion (lateral pelvic tilt) which occurs in case of hip abduction[34] and indicates a generic, though important, good-practice rule.

For all methods analysed, the HJC determination errors increased with the amplitude of the HJC displacement; however, the error sensitivity to pelvic motion varied among methods. The dUKF method was shown to be the least sensitive to pelvic movement, as confirmed by the Pearson correlation analysis. dUKF also showed the smallest HJC median errors for the *StarArc* (5.2 mm, that is median femoral deviation of 0.8° assuming 350 mm femoral length) compared to the other methods, with an error reduction of about 30%. The performance of all the other methods (MAP, PIV, PSF and UKF) was found to be comparable, thus all equally affected by the unknown passive pelvic motion. Although the slight improvement obtained with the dUKF method in terms of median femoral deviation (about 0.3°) with respect to the clinical requirements, dUKF methods potentially allow limitating the median femoral deviation ($< 1°$) in the case of larger pelvic displacements. As summarized in Table 3, the errors computed in this study for the PIV and MAP methods in correspondence to the *StarArc* movement are in agreement with the results reported for comparable ranges of pelvic motions in previous studies.[15,21] The localization errors of the PIV methods are increased by 3 times (median value equal to 7.9 mm) with respect to the case in which no pelvic motion occurs (mean/median value below 3 mm),[16,17,19] thus confirming that this source of error highly affects the estimation of the HJC as previously stated.[21] As regarding the MAP method, the HJC localization errors resulted in this work (median error equal to 9.5 mm) were slightly larger than those reported in Picard et al.[12] (maximum error equal to 8 mm, assuming 350 mm femoral length), probably due to different executions of the femoral manoeuvres performed on the subjects during which the pelvic motion was not measured.

In the case of HJC localization computed using the quasi-planar movements ($ROT_{1,2,3,4}$), it should be noted that these movements are better suited for the determination of an axis of rotation rather than a centre of rotation and therefore should not be employed separately for the functional determination of the HJC.[19,20] These movements were included in the analysis to obtain pooled datasets characterized by different pelvic displacement amplitudes (small, medium and large), which allowed investigation of the methods' robustness. A detailed definition of the best hip pivoting movement,

Table 3. Localization errors of the five HJC estimation methods analysed in this work (last row, results given in boldface) are compared to previous literature results.

Set-up	Pelvic motion (mm)	PIV (mm)	MAP (mm)	PSF (mm)	UKF (mm)	dUKF (mm)
Whole-body cadavers[12]	?		< 8.0*			
Simulation[13]	Y (< 16)		< 6.1*			
Mechanical linkage[15]	Y (15)		11.7 (mean)			
Hemi-corpses[16]	N	2.41 ± [2.0; 2.9] (median ± quartiles)				
Hemi-corpses[17]	N	2.7 ± 2.9 (mean ± SD)				
Mechanical linkage[19]	N	2.7 ± 0.4 (mean ± SD)		7.0 ± 4.0 (mean ± SD)		
Whole-body cadavers[18]	?			< 32.7		
Hip phantom[21]	Y (2.5–8)	6 ± [0.5; 7.5] (median ± quartiles)			3.5 ± [1.5; 2.5] (median ± quartiles)	
Whole-body cadavers	**Y** (1–9)	**7.9 ± [2.5; 0.4]** (median ± quartiles)	**9.5 ± [0.7; 0.7]** (median ± quartiles)	**9.2 ± [3.2; 6.2]** (median ± quartiles)	**8.7 ± [2.8; 2.3]** (median ± quartiles)	**5.2 ± [1.2; 1]** (median ± quartiles)

PIV: pivoting; MAP: minimal amplitude point; PSF: sphere fitting; UKF: unscented Kalman filter; dUKF: dual unscented Kalman filter; SD: standard deviation; HJC: hip joint centre.
The experimental set-up (first column) is specified for each work, as well as information on whether the pelvic motion occurs or not (second column: yes (Y); no (N); yes but measurements are not reported (?)).
*Specifies that the HJC localization errors were derived from the angular deviation (assuming a 350 mm femoral length) as reported in the original papers.

both in terms of type and amplitude, for the functional HJC determination in CAOS set-up is beyond the scope of this study and warrants further research.

A limitation of this study is that no real pelvic skin marker was available in the experimental set-up, so the observations of the pelvic point *A* were indirectly obtained through the simulation of STAs in the area of a calibrated anatomical landmark. It is well known that STA is both task and subject dependent.[35] Although body mass index (BMI) and skinfold thickness were shown to be important factors to describe the relation between internal and external pelvic landmarks,[36] their correlation effects[37] are usually neglected when modelling the skin marker displacements during body segments' movements. Joint kinematics[28] or rigid-body motion[38] driven models were proposed to estimate the STA on thigh skin markers, but to the best of the authors' knowledge, no studies have been performed on pelvic skin markers.[39] In this work, a joint kinematic–driven model with randomly sampled correlation coefficients is used to simulate the STA of a skin marker placed on the contralateral ASIS, supposed to be minimal as it is far away from the moving joint. In this location, the skin marker displacements quantified *in vivo* with static standing poses were reported as negligible (< 1 mm) during hip flexion (until 90°)[40] for 20 healthy subjects with BMI fluctuating in the normal range ($22.8 \pm 2.7\,kg/m^2$). In order to simulate a worst-case scenario as expected for subjects with higher BMI, the maximum amplitude of the simulated STA on the observed point *A* was increased by 500% (set to 5 mm) with respect to the one quantified by Hara et al.[40]

Thanks to the a priori statistical model of the measurement noise in the HJC estimation process,[23] HJC estimation methods based on a Kalman filter are supposed to compensate any possible STA better than the PSF method, although a model of the STA was not explicitly added to the state filter model. It has to be noted that the high HJC localization errors found for the UKF method can be explained by the inability of the filter to distinguish between the actual pelvic motion and the marker displacement due to the simulated STAs. On the contrary, the global optimization process allows the dUKF method to partially compensate for STA on the pelvic marker position and provide a better HJC estimate. The dUKF method was shown to be robust to a simulated additive noise correlated to the hip joint angles with 5 mm amplitude.

Conclusion

An innovative HJC estimation method, based on a dUKF algorithm specifically designed for CAOS applications, is proposed to reduce the estimation errors due to the unavoidable and untracked pelvic motions that occur during passive femoral manoeuvres. These motions were quantified in the range between 0.1 and 15 mm using an *in vitro* set-up that reproduced a

realistic surgical scenario, thus showing that pelvic motions actually occur especially during the largest hip abductions. The dUKF proved to be the least sensitive method to pelvic movements, increasing HJC localization accuracy by 30% for HJC displacements >6 mm during multi-planar motions, and to be robust to simulated pelvic STAs. Further tests to quantify and possibly model the STAs of skin markers placed on the hip segment during femoral pivoting motions need to be addressed in the future. Moreover, the method will be further developed in order to improve its applicability in a surgical context, such as optimizing the algorithm's implementation thus reducing its computational time.

Acknowledgements

The authors wish to thank Dr Marco Donati and Dr Fabrizio Margheritini of the Università degli Studi di Roma Foro Italico for their support in performing the experiments and in processing the data.

Declaration of conflicting interests

The authors declare that there is no conflict of interest.

Funding

This research received no specific grant from any funding agency in the public, commercial, or not-for-profit sectors.

References

1. Cereatti A, Camomilla V, Vannozzi G, et al. Propagation of the hip joint centre location error to the estimate of femur vs pelvis orientation using a constrained or an unconstrained approach. *J Biomech* 2007; 40(6): 1228–1234.
2. Della Croce U, Leardini A, Chiari L, et al. Human movement analysis using stereophotogrammetry. Part 4: assessment of anatomical landmark misplacement and its effects on joint kinematics. *Gait Posture* 2005; 21(2): 226–237.
3. Arbabi E, Schmid J, Boulic R, et al. Sensitivity of hip tissues contact evaluation to the methods used for estimating the hip joint center of rotation. *Med Biol Eng Comput* 2012; 50: 595–604.
4. Alazzawi S, Field MH, Bardakos NV, et al. The position of the centre of the femoral head relative to the midline of the pelvis: a consistent landmark in total knee replacement surgery. *Knee* 2012; 19(6): 827–831.
5. Hill JC, Salazar-Torres JJ, Orr JF, et al. A low-cost solution for the restoration of femoral head centre during total hip arthroplasty. *Proc IMechE, Part H: J Engineering in Medicine* 2013; 227(6): 629–635.
6. Haaker RG, Stockheim M, Kamp M, et al. Computer-assisted navigation increases precision of component placement in total knee arthroplasty. *Clin Orthop Relat R* 2005; 433: 152–159.
7. Cereatti A, Margheritini F, Donati M, et al. Is the human acetabulofemoral joint spherical? *J Bone Joint Surg* 2010; 92(2): 311–314.
8. Camomilla V, Cereatti A, Vannozzi G, et al. An optimized protocol for hip joint centre determination using the functional method. *J Biomech* 2006; 39(6): 1096–1106.
9. Cappozzo A. Gait analysis methodology. *Hum Movement Sci* 1984; 3(1–2): 27–50.
10. Ehrig RM, Taylor WR, Duda GN, et al. A survey of formal methods for determining the centre of rotation of ball joints. *J Biomech* 2006; 39(15): 2798–2809.
11. Jaramaz B, Hafez MA and DiGioia AM. Computer-assisted orthopaedic surgery. *Proc IEEE* 2006; 94(9): 1689–1695.
12. Picard F, Leitner F, Gregori A, et al. A cadaveric study to assess the accuracy of computer-assisted surgery in locating the hip center during total knee arthroplasty. *J Arthroplasty* 2007; 22(4): 590–595.
13. Stindel E. Detection of the center of the hip joint in computer-assisted surgery: an evaluation study of the Surgetics algorithm. *Comput Aided Surg* 2005; 10(3): 133–139.
14. Marin F, Mannel H, Claes L, et al. Accurate determination of a joint rotation center based on the minimal amplitude point method. *Comput Aided Surg* 2003; 8(1): 30–34.
15. Lustig S, Fleury C, Servien E, et al. The effect of pelvic movement on the accuracy of hip centre location acquired using an imageless navigation system. *Int Orthop* 2011; 35: 1605–1610.
16. De Momi E, Lopomo N, Cerveri P, et al. In-vitro experimental assessment of a new robust algorithm for hip joint centre estimation. *J Biomech* 2009; 42(8): 989–995.
17. Lopomo N, Sun L, Zaffagnini S, et al. Evaluation of formal methods in hip joint center assessment: an in vitro analysis. *Clin Biomech* 2010; 25(3): 206–212.
18. Mihalko WM, Phillips MJ, Fishkin Z, et al. Pelvic tracker effects on hip center accuracy using imageless navigation. *Comput Aided Surg* 2006; 11(4): 214–218.
19. Siston RA and Delp SL. Evaluation of a new algorithm to determine the hip joint center. *J Biomech* 2006; 39(1): 125–130.
20. Gamage SSH and Lasenby J. New least squares solutions for estimating the average centre of rotation and the axis of rotation. *J Biomech* 2002; 35(1): 87–93.
21. De Momi E, Beretta E and Ferrigno G. Hip joint centre localisation with an unscented Kalman filter. *Comput Methods Biomech Biomed Engin* 2013; 16(12): 1319–1329.
22. Sitz A, Schwarz U and Kurths J. The unscented Kalman filter, a powerful tool for data analysis. *Int J Bifurcat Chaos* 2004; 14(6): 2093–2105.
23. Haykin SS. Dual extended Kalman filter methods. In: Haykin SS (ed.) *Kalman filtering and neural networks*. New York: Wiley, 2001, pp.123–170.
24. Julier SJ and Uhlmann JK. Unscented filtering and nonlinear estimation. *Proc IEEE* 2004; 9(3): 401–422.
25. Tsallis C and Stariolo D. Generalized simulated annealing. *Phys A* 1996; 233(1–2): 395–406.
26. Cereatti A, Donati M, Camomilla V, et al. Hip joint centre location: an ex vivo study. *J Biomech* 2009; 42(7): 818–823.
27. Grimpampi E, Camomilla V, Cereatti A, et al. Metrics for describing soft tissue artefact and its effect on pose, size and shape of marker clusters. *IEEE Trans Biomed Eng* 2014; 61(2): 362–367.

28. Camomilla V, Cereatti A, Chèze L, et al. A hip joint kinematics driven model for the generation of realistic thigh soft tissue artefacts. *J Biomech* 2013; 46(3): 625–630.
29. Söderkvist I and Wedin PA. Determining the movements of the skeleton using well-configured markers. *J Biomech* 1993; 26(12): 1473–1477.
30. Cappozzo A, Catan F, Della Croce U, et al. Position and orientation in space of bones during movements: anatomical frame definition and determination. *Clin Biomech* 1995; 10(4): 171–178.
31. Jolliffe IT. *Principal component analysis*. New York: John Wiley & Sons, 2005, p.5.
32. Koyonos L, Stulberg SD, Moen TC, et al. Sources of error in total knee arthroplasty. *Orthopedics* 2009; 32(5): 317.
33. Rodriguez Y, Baena F, Hawke T, et al. A bounded iterative closest point method for minimally invasive registration of the femur. *Proc IMechE, Part H: J Engineering in Medicine* 2013; 227(10): 1135–1144.
34. Kapandji IA. *The physiology of the joints: lower limb*, vol. 2. London: Churchill Livingstone, 1988.
35. Leardini A, Chiari L, Della Croce U, et al. Human movement analysis using stereophotogrammetry. Part 3: soft tissue artefact assessment and compensation. *Gait Posture* 2005; 21(2): 212–225.
36. Lalonde NM, Dansereau J, Lacoste M, et al. Modelling skin pelvic landmark coordinates into corresponding internal bone for wheelchair users. *IEEE Trans Biomed Eng* 2007; 54(1): 11–18.
37. Barre A, Thiran JP, Jolles B, et al. Soft tissue artefact assessment during treadmill walking in subjects with total knee arthroplasty. *IEEE Trans Biomed Eng* 2013; 60(11): 3131–3140.
38. Andersen M, Damsgaard M, Rasmussen J, et al. A linear soft tissue model for human movement analysis: proof of concept using in vivo data. *Gait Posture* 2012; 35: 609–611.
39. Peters A, Galna B, Sangeux M, et al. Quantification of soft tissue artifact in lower limb human motion analysis: a systematic review. *Gait Posture* 2010; 31: 1–8.
40. Hara R, Sangeux M, Baker R, et al. Quantification of pelvic soft tissue artifact in multiple static positions. *Gait Posture* 2013; 39(2): 712–717.
41. Vaccarella A, De Momi E, Enquobahrie A, et al. Unscented Kalman filter based sensor fusion for robust optical and electromagnetic tracking in surgical navigation. *IEEE T Instrum Meas* 2012; 62(7): 2067–2081.
42. Vaccarella A, De Momi E, Valenti M, et al. Application of unscented Kalman filter for robust pose estimation in image-guided surgery. *P SPIE Med Imag* 2012; 8316: 1–6.
43. Fioretti S and Jetto L. Accurate derivative estimation from noisy data: a state space approach. *Int J Syst Sci* 1989; 20(1): 33–53.

Appendix 1

State space model

A discrete-time state-space model is used

$$\mathbf{x}_{k+1} = f(\mathbf{x}_k, \mathbf{v}_k) \tag{2}$$

$$\mathbf{y}_k = h(\mathbf{x}_k, \mathbf{p}, \mathbf{e}_k) \tag{3}$$

where $\mathbf{x}_k$ is the state vector, $\mathbf{y}_k$ is the observations vector, $\mathbf{v}_k$ and $\mathbf{e}_k$ are the process and measurement noise, respectively, and $\mathbf{p}$ is the parameter vector. f and h are the non-linear state transition and measurement functions, respectively.

The state vector $\mathbf{x}$ includes the time-variant variables of the hip kinematic model with their first-order dynamics

$$\mathbf{x} = \begin{bmatrix} {}^{H}\mathbf{q}_L & {}^{H}\omega_L & {}^{H}\mathbf{c}_L & {}^{H}\dot{\mathbf{c}}_L & \vartheta & \dot{\vartheta} & \eta & \dot{\eta} \end{bmatrix} \tag{4}$$

where ${}^{H}\mathbf{c}_L$ and ${}^{H}\mathbf{q}_L$ are the translational and rotational (quaternion-based convention) components of the TF_H frame expressed in the TF_L, respectively; ${}^{H}\omega_L$ is the vector of the angular velocities of the TF_H in the TF_L,[41,42] and (ϑ, η) are the angular components of the spherical coordinates that describe the position of point A in the TF_H (${}^{A}\mathbf{c}_H$) with their relative derivatives $(\dot{\vartheta}, \dot{\eta})$.

The process noise $\mathbf{v}_k$ is assumed to be drawn from a multivariate normal distribution $N(0, \mathbf{Q})$ with covariance $\mathbf{Q}$. In the numerical differentiation approach, the state transition function for a state variable $x_v \in \mathbf{x}$ can be specified as a first-order Taylor series expansion

$$\begin{bmatrix} x_v(k+1) \\ \dot{x}_v(k+1) \end{bmatrix} = \begin{bmatrix} 1 & dt \\ 0 & 1 \end{bmatrix} \cdot \begin{bmatrix} x_v(k) \\ \dot{x}_v(k) \end{bmatrix} + \begin{bmatrix} 0 \\ v(k) \end{bmatrix} \tag{5}$$

where dt is the sampling time interval. According to Fioretti and Jetto,[43] the covariance matrix $\mathbf{Q}_v$ of each state variable is

$$\mathbf{Q}_v = \begin{bmatrix} \frac{dt^3}{3} & \frac{dt^2}{2} \\ \frac{dt^2}{2} & dt \end{bmatrix} \cdot \sigma^2_{Q,v} \tag{6}$$

where $\sigma^2_{Q,v}$ is an a priori set according to the frequency content of the signal and the sampling frequency. The values ($\sigma^2_{Q,q_{\alpha,\beta,\gamma}}$ $\sigma^2_{Q,\omega}$ $\sigma^2_{Q,{}^{H}c_L}$ $\sigma^2_{Q,\vartheta,\eta}$), which define the covariance of the state process noise, are reported in Table 4.

The observation vector $\mathbf{y}$ is

$$\mathbf{y} = \begin{bmatrix} {}^{F}\mathbf{c}_L & {}^{F}\mathbf{q}_L & {}^{A}\mathbf{c}_L \end{bmatrix} \tag{7}$$

where ${}^{F}\mathbf{c}_L$ is the position of the TF_F origin in the laboratory frame, ${}^{F}\mathbf{q}_L$ is the quaternion describing the orientation of the TF_F in the laboratory technical frame, and ${}^{A}\mathbf{c}_L$ is the three-dimensional position of the pelvic point A in the TF_L.

The measurement noise $\mathbf{e}_k$ is supposed to be isotropic and is described by the covariance matrix $\mathbf{R}$. The values ($\sigma^2_{R,q_{\alpha,\beta,\gamma}}$ $\sigma^2_{R,{}^{F}\mathbf{c}_L}$ $\sigma^2_{R,{}^{A}\mathbf{c}_L}$), which define the covariance of the measurement noise, were set in relation to the target registration errors computed on the femoral technical frame and on the calibrated contralateral ASIS (see Table 4).

The vector $\mathbf{p}$ includes the time-invariant parameters of the hip kinematic model, that is, the HJC position in the TF_F and the distance ρ between the HJC and the pelvic point A

Table 4. Values of the covariance matrices of the dual unscented Kalman filter algorithm.

Process noise covariance (**Q**)		Measurement noise covariance (**R**)		Parameter noise covariance (**S**)		Initial state covariance ($\mathbf{P_0}$)	
$\sigma^2_{Q,q_{\alpha,\beta,\gamma}}$ *	10^{-8} rad^2	$\sigma^2_{R,q_{\alpha,\beta,\gamma}}$ *	2.5×10^{-7} rad^2	$\sigma^2_{S,{}^H\mathbf{c}_F}$	2×10^{-1} mm^2	$\sigma^2_{P_0,q_{\alpha,\beta,\gamma}}$ *	10^{-8} rad^2
$\sigma^2_{Q,\omega}$	10^{-10} mm^2/s^2	$\sigma^2_{R,{}^F\mathbf{c}_L}$	10^{-2} mm^2	$\sigma^2_{S,\rho}$	2×10^{-1} mm^2	$\sigma^2_{P_0,\omega}$	10^{-10} mm^2/s^2
$\sigma^2_{Q,{}^H\mathbf{c}_L}$	10^{-1} mm^2	$\sigma^2_{R,{}^A\mathbf{c}_L}$	10^{-1} mm^2			$\sigma^2_{P_0,{}^H\mathbf{c}_L}$	1 mm^2
$\sigma^2_{Q,\vartheta,\eta}$	10^{-4} rad^2					$\sigma^2_{P_0,\vartheta,\eta}$	10^{-4} rad^2

*The noise vector of rotational variables expressed in quaternion convention is modelled with a three-component vector representing noise about *x*, *y*, and *z* rotation axes.[41,42]

Table 5. Values of the parameters of the simulated annealing and optimization process.

Simulated annealing		$\mathbf{S_0}$		Optimization process	
λ	0.998	$\sigma^2_{S_0,{}^H\mathbf{c}_F}$	30 mm^2	H	40
δ	10^{-7}	$\sigma^2_{S_0,\rho}$	30 mm^2	$O_{\min}$	1 mm

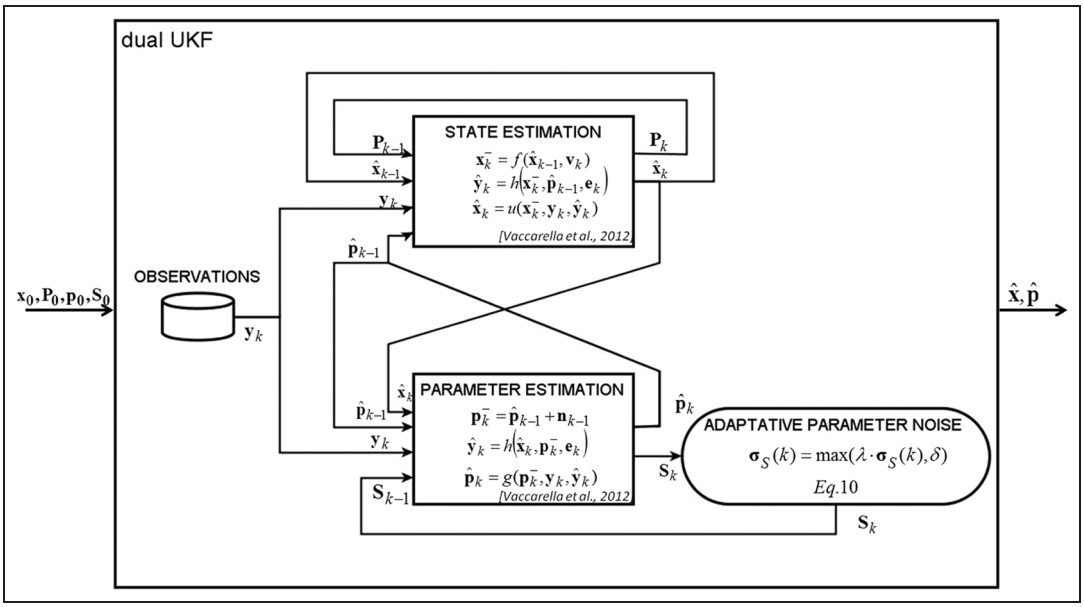

Figure 6. Schematic of the dUKF: the dual filtering approach with simulated annealing.
UKF: unscented Kalman filter.

$$\mathbf{p} = \begin{bmatrix} {}^H\mathbf{c}_F & \rho \end{bmatrix} \tag{8}$$

and it is defined as a stationary process driven by process noise $\mathbf{n}_k$, as follows

$$\mathbf{p}_{k+1} = \mathbf{p}_k + \mathbf{n}_k \tag{9}$$

The parameter process noise $\mathbf{n}_k$ is a zero-mean Gaussian distribution $N(0, \mathbf{S})$, where $\mathbf{S}$ is the covariance matrix. The values $\boldsymbol{\sigma}^2_S = (\sigma^2_{S,{}^H\mathbf{c}_F} \quad \sigma^2_{S,\rho})$, which define the covariance of the process noise for each parameter, are reported in Table 4.

Two UKFs[23,24] are used to compute the update of the state vector $\hat{\mathbf{x}}_k$ and of the state covariance $\mathbf{P}_k$ in the state estimation step and the update of the parameter vector $\hat{\mathbf{p}}_k$ and of the parameter covariance $\mathbf{S}_k$ in the parameter estimation step, as shown in Figure 6.

The simulated annealing method[25] is used to adapt the parameter covariance matrix $\mathbf{S}$ during the dual filtering process, as shown in Figure 6. Each value of the parameter covariance $\boldsymbol{\sigma}^2_S$ is updated at each time frame $k = 1, ..., N$, as

$$\boldsymbol{\sigma}_S(k) = \max(\lambda \cdot \boldsymbol{\sigma}_S(k), \delta) \tag{10}$$

where λ and δ are annealing parameters (values in Table 5).

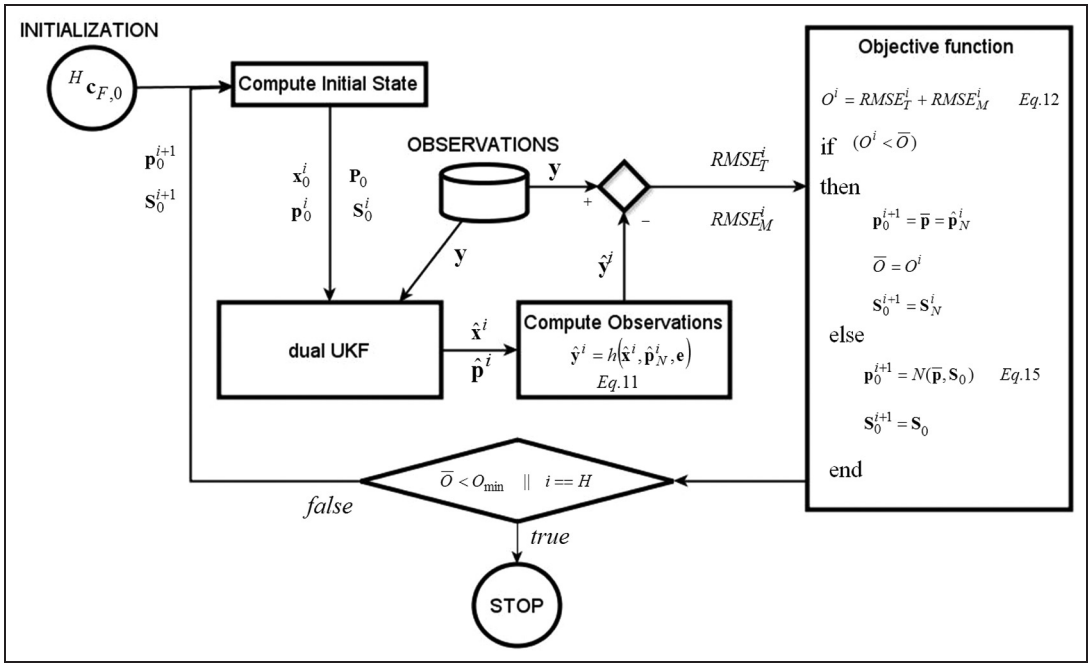

Figure 7. Schematic of the enhanced dUKF: the global optimization problem in the parameter space.
UKF: unscented Kalman filter.

Enhanced dUKF

In order to globally search the optimal solution in the parameter space, the dual UKF is iteratively computed, as shown in Figure 7. At the end of the dual estimation process, the estimated observation vector $\hat{\mathbf{y}}^i$ is computed evaluating the measurement function (3) on the last estimate of the parameter vector

$$\hat{\mathbf{y}}^i = h\left(\hat{\mathbf{x}}^i, \hat{\mathbf{p}}_N^i, \mathbf{e}\right) \tag{11}$$

where $i = 1, \ldots, H$ is the iteration number of the optimization process. The objective function (O) to be minimized is the sum of the root mean square errors between the actual observations $\mathbf{y}$ and the estimated observation $\hat{\mathbf{y}}^i$

$$\min_{\mathbf{p}} O^i = \min_{\mathbf{p}}\left(RMSE_T^i + RMSE_M^i\right) \tag{12}$$

$$RMSE_T^i = \sqrt{\frac{\sum_{k=1}^{N}\left\|{}^{F}\hat{\mathbf{c}}_{L,k}^i - {}^{F}\mathbf{c}_{L,k}\right\|^2}{N}} \tag{13}$$

$$RMSE_M^i = \sqrt{\frac{\sum_{k=1}^{N}\left\|{}^{A}\hat{\mathbf{c}}_{L,k}^i - {}^{A}\mathbf{c}_{L,k}\right\|^2}{N}} \tag{14}$$

If $\hat{\mathbf{p}}_N^i$ corresponds to the current minimum of the cost function ($\bar{O}$), the next dual filtering iteration would be initialized using the current adaptive parameter noise covariance $\mathbf{S}_N^i$. Otherwise, a new parameter vector $\mathbf{p}_0^{i+1}$ is generated as

$$\mathbf{p}_0^{i+1} = \mathrm{N}(\bar{\mathbf{p}}, \mathbf{S}_0) \tag{15}$$

where $\bar{\mathbf{p}}$ is the parameter solution corresponding to the current minimum of the objective function and $\mathbf{S}_0$ is the initial parameter covariance matrix, whose ($\sigma^2_{S_0,{}^{H}\mathbf{c}_F}$ $\sigma^2_{S_0,\rho}$) values are reported in Table 5. The optimization process stops when the objective function is evaluated below a threshold ($O_{\min}$) or when the maximum number of iterations H is reached (see Table 5).

The dUKF algorithm was initialized using the position of the HJC in the $\mathrm{TF_F}$ ($^{H}\mathbf{c}_{F,0}$) estimated using Siston and Delp.[19] The initial state vector $\mathbf{x}_0$ and parameter ρ_0 are derived from the observations relative to the first-time frame, while the first derivatives of the state vector were set equal to 0.[21] Values of the initial state covariance matrix $\mathbf{P}_0$($\sigma^2_{P_0,q_{\alpha,\beta,\gamma}}$ $\sigma^2_{P_0,\omega}$ $\sigma^2_{P_0,{}^{H}\mathbf{c}_L}$ $\sigma^2_{P_0,\vartheta,\eta}$) are reported in Table 4.